N. Vedavathi, Ghuram Dharmaiah, Kothuru Venkatadri, and Shaik Abdul Gaffar*

Numerical study of radiative non-Darcy nanofluid flow over a stretching sheet with a convective Nield conditions and energy activation

https://doi.org/10.1515/nleng-2021-0012
Received Dec 19, 2020; accepted Apr 14, 2021.

Abstract: Numerous industrial processes such as continuous metal casting and polymer extrusion in metal spinning, include flow and heat transfer over a stretching surface. The theoretical investigation of magnetohydrodynamic thermally radiative non-Darcy Nanofluid flows through a stretching surface is presented considering also the influences of thermal conductivity and Arrhenius activation energy. Buongiorno's two-phase Nanofluid model is deployed in order to generate Thermophoresis and Brownian motion effects [1]. By similarity transformation technique, the transport equations and the respective boundary conditions are normalized and the relevant variable and concerned similarity solutions are presented to summarize the transpiration parameter. An appropriate Matlab software (Bvp4c) is used to obtain the numerical solutions. The graphical influence of various thermo physical parameters are inspected for momentum, energy and nanoparticle volume fraction distributions. Tables containing the Nusselt number, skin friction and Sherwood number are also presented and well argued. The present results are compared with the previous studies and are found to be well correlated and are in good agreement. The existing modelling approach in the presence of nanoparticles enhances the performance of thermal energy thermoplastic devices.

Keywords: Buongiorno's two-phase Nanofluid model, Arrhenius activation energy, non-Darcy, radiation, magnetohydrodynamics, velocity slip, Biot number

1 Introduction

Nanofluids are maneuvered by suspending nanoparticles with average size below 100 nm in traditional heat transfer fluids such as ethylene glycol, oil and water. An important role is simulated by thermal conductivity of water, oil and ethylene glycol with nanoparticles in the heat transfer between the heat and mass transfer medium and the heat and mass transfer surface. The rise in thermal conductivity is substantial in improving the heat transfer behavior of the fluids. High heat transfer performance is necessitated by several engineering applications. In several engineering and industrial applications, the thermal conductivity of nanofluid is not constant and it differs linearly with temperature. Nanofluid is the combination of nanoparticles with water. The addition of a surfactant to a base fluid improves thermal conductivity and convective heat transfer. Nanofluid technology has emerged as a modern heat transfer technique that is more effective. Nanofluids are used in solar energy applications such as heat exchanger design, medical applications such as cancer therapy and safer surgery by heat treatment applications. Nanofluid technology can be used to create better oil and lubricants for realistic applications [2]. Many scientists and engineers have been working on fluid forming for the past few decades in order to improve efficiency for various thermal applications. The term "nanofluid" has been proposed to address the new heat transfer problems by applying nanotechnology to heat transfer [3]. Many authors have predicted that nanofluids would have greater convective heat

N. Vedavathi, Department of Mathematics, Koneru Lakshmaiah Education Foundation, Vaddeswaram, India
Ghuram Dharmaiah, Department of Mathematics, Narasaraopeta Engineering College, Yellamanda, India
Kothuru Venkatadri, Department of Mathematics, Sreenivasa Institute of Technology and management studies, Chittoor, India
***Corresponding Author: Shaik Abdul Gaffar,** Department of Information Technology, Mathematics Section, University of Technology and Applied Sciences, Salalah, Oman, E-mail: abdulsgaffar0905@gmail.com

transfer capabilities than base fluids. Heat and mass transfer of nanofluids have integrated many practical applications of thermal and solutal stratification. Patil *et al.* [4] investigated the unsteady mixed convection nanoliquid flows through an exponentially stretching surface in the presence of applied transverse magnetic field with realistic application to solar systems. Khan *et al.* [5] presented the entropy analysis and gyrotactic microorganisms of Buongiorno's nanofluid between two stretchable rotating disks using homotopy analysis. Nainaru *et al.* [6] studied the effects of heat transfer characteristics on 3D MHD flows of nanofluid induced by stretching surface with thermal radiation. They observed a rise in the fluid temperature and velocity with a rise in variable thermal conductivity. Shiriny *et al.* [7] considered the forced convection flow of nanofluid in a horizontal microchannel with cross flow injection and slip velocity on microchannel walls. They observed that an increase in velocity slip and heat transfer rate by increasing the angle of injection to 94°. Suhail and Siddiqui [8] presented the numerical study the natural convection flows of nanofluid within a vertical annulus. They discussed the simulations for various nanoparticle concentrations for various heat flux values. Few recent studies on nanofluid includes [9–11].

Due of its universal and practical applications, the convective boundary layer plays an important role in the process of heat supply to the fluid via a particle surface with a restricted heat efficiency, especially in various manufacturing and advanced processes that include transpiration cooling, fabric cleaning, laser pulse heating and so on. Convective heat transfer is important in mechanisms like thermal insulation, gas turbines and nuclear power stations among others [11]. The analysis of electrically conducting fluids like sea water, antioxidants, plasma and metal oxides is known as magnetohydrodynamics (MHD). Alfven [12] was the one who invented the word MHD. The strength of magnetic induction affects MHD. The MHD fluid flows has a many engineering and industrial applications like crystal development, nuclear freezing, magnetic improved drug, MHD detectors, and energy production. The MHD fluid flows also has many applications in healthcare and biopharmaceutical fields such as hyperglycemia and emergency medicine, radiation therapy and many more. Khilap *et al.* [13] assessed the melting heat transfer and non-uniform heat source on magnetic nanofluid flows past a porous cylinder using Keller box technique. Jha and Malgwi [14] analyzed the mixed MHD convection flow of viscous fluid in a vertical microchannel considering the effects buoyancy forces, pressure gradient, Hall and Ionslip current. Haque [15] explored the effects of induced magnetic field and heat sink on the micropolar fluid flows past a semi-infinite vertical porous plate using the explicit finite difference technique. They observed that both heat sink and thermal diffusion have a growing effect of the species concentration and the lighter particles have a higher fluid concentration compared to heavier ones. Alam *et al.* [16] considered the principles of magnetohydrodynamics and ferrohydrodynamics to examine the biomagnetic flows of blood containing gold nanoparticles past a stretching surface in the presence of Biot number, suction and velocity slip using the bvp4c technique. Khan *et al.* [17] presented the entropy analysis of MHD radiative flows of Jeffrey fluid past an inclined surface using Keller-Box technique. Vedavati *et al.* [18] examined the MHD convection flows of nanofluid past an inverted cone considering the suction/injection effects and entropy analysis is also presented.

Thermal radiation is a key aspect in many engineering processes that take place at extreme temperatures. Many industrial applications involving extreme temperatures such as gas turbines, nuclear power stations and various combustion turbines for aircraft, rockets, spacecraft and aerospace engineering have stressed the effects of radiation on convection. Radiative heat transfer is crucial in oxidation, fossil fuel energy cycles, astrophysical flows, renewable energy engineering are the other applications. Mumtaz *et al.* [19] studied the mixed convective chemically radiative flows of tangent hyperbolic fluid with viscous dissipation in a doubly stratified medium using BVPh2 scheme. Yusuf *et al.* [20] investigated the entropy analysis on radiative MHD flows of Williamson nanofluid past an inclined porous plate considering the chemical reaction, gyrotactic microorganisms and convective heat transfer effects. Jawad *et al.* [21] presented the radiative MHD flows of second grade hybrid nanofluid past a stretching/shrinking surface using the homotopy analysis. They observed that an increase in the volume fraction of the nanoparticles increases the fluid's thermal efficiency. Ge-JiLe *et al.* [22] discussed the radiative MHD flows of Jeffrey fluid past the horizontal walls in the porous medium and considering the viscous dissipation effects. Jawad *et al.* [23] considered the MHD mixed convection flows of Maxwell nanofluid past a stretching surface considering the influences of variable thermal conductivity, gyrotactic microorganisms, radiation, Dufour and Soret.

A surface will fluid-filled pores (voids) is termed as porous media. In industry, porous materials are commonly seen in reverse osmosis, steam turbines, heterogeneous catalysts, activated carbon columns, filtration centers and evaporative freezing. The analysis of fluid flow processes in a porous media has sparked researcher's interest due to its various implications in scientific, bio-

logical and industrial producing goods such as porous bearings, atomic reservoirs, groundwater contamination, crude oil processing, casting and welding in production processes, porous bearing, hydro power, vapor movement in fibrous packaging, organic catalytic reactors, renewable energy and recycling devices. In 1856, Darcy formulated a principle that states that the volumetric flux of fluid across a medium has a direct relationship with the pressure gradient. Practically, the Darcy term [24] is commonly used in the problems relating to flow saturating porous space modeling and analysis. The Darcy's law is only applicable when the velocity is low and the porosity is small. Inertia and boundary impacts are ignored by this rule. The customized version of classical Darcy's principle results in the non-Darcian porous space which integrates inertial and boundary impacts. As a result, Forchheimer [25] took into account the inertia by using a square velocity term in the momentum term. Non-Darcian versions are extensions of the standard Darcy concept that includes inertial drag, vorticity dispersion and combinations of these impacts. Darcy law in the Darcian medium is criticized as failing at high velocity, high porosity medium and enormous Reynolds number. To take the responsibility of the inertia impacts of pressure drop, the Forchheimer expression is integrated into the square velocity term within the momentum equation during this method. Pop and Ingham [26] and Vafai [27] surveyed temperature change in heat and mass transfer flows of Darcian and non-Darcian porous media. Hayat *et al.* [28] presented the Darcy-Forchheimer 3D flows of nanofluid past a rotating surface considering the effects of activation energy and heat generation/absorption using NDsolve technique. Asma *et al.* [29] examined the convective heat transfer analysis of Darcy-Forchheimer 3D flows of nanofluid past a rotating disk in the presence of Arrhenius activation energy using shooting technique. Ramzan *et al.* [30] investigated the melting heat transfer effects of unsteady nanofluid flow between two parallel disks considering the Darcy-Forchheimer permeable media, Cattaneo-Christov heat flux ad homogeneous-heterogeneous reactions using bvp4c technique. Sohail *et al.* [31] studied the MHD convection flows of hybrid nanofluid past a stretching porous surface with viscous dissipation impacts using successive over relaxation technique. Kareem and Abdulhadi [32] investigated the axisymmetric MHD Darcy-Forchheimer flows of third grade fluid past a stretching cylinder considering the Cattaneo-Christov effects using homotopy analysis technique. Jawad *et al.* [33] presented the entropy analysis of MHD radiative Darcy-Forchheimer 3D Casson nanofluid flows past a turning disk considering the Arrhenius activation energy using homotopy analysis scheme. Zhang *et al.* [34] MHD Darcy-Brinkman-Forchheimer flows of third-grade fluid between two parallel plates considering the influences of Joule heating and viscous dissipation.

Many scientists and engineers have considered the activation energy, which was originally proposed by Svante Arrhenius in 1889 and is defined as the minimum amount of energy needed to carry out a reaction phase. The activation energy is the energy given to the reactants to transform them into products in different chemical reactions. The kinetic and potential energy involved with the molecules are of deemed importance to break bonds or stretch and twist bonds. It is observed that molecules rebound with each other without completion of reaction if their movement is detected slowly with low kinetic energy or they smash improperly. However, due to high momentum energy, a chemical reaction is initiated for which minimum activation energy is required. The activation energy concept is more significant in suspension of oil, hydrodynamics, oil storage industries and in geothermal. Owing to such interesting applications, this phenomenon is studied by many researchers. For instance, Umair *et al.* [35] explored the impacts of Soret and Dufour on chemically radiative magnetohydrodynamics flows of Cross liquid through a shrinking/stretching wedge also considering the effects of activation energy. Aldabesh *et al.* [36] dealt with the unsteady flow of Williamson nanofluid with gyrotactic microorganisms through a rotating cylinder considering the impacts of activation energy, chemical reaction and variable thermal conductivity. Mehboob *et al.* [37] investigated the MHD thermally radiative 3D flows of Cross fluid considering the effects convective heat transfer, stratification phenomena, heat source/sink and activation energy using bvp4c technique. Sami *et al.* [38] explored effects of velocity slip and Arrhenius activation energy on MHD radiative 3D rheology of Eyring-Powell nanofluid past a stretching surface using shooting technique. Muhammad *et al.* [39] studied the effects of Brinkman number, magnetic parameter, diffusion parameter, Weissenberg number and activation energy on the entropy analysis of Carreau-Yasuda fluid past a stretching surface using the homotopy analysis method. Few recent studies on activation energy include [40–42].

By keeping the above studies in mind, the main objective of the current analysis is to study the effects of Arrhenius activation energy of Darcy-Forchheimer Nanofluid past a stretching surface in the presence of thermal radiation and magnetohydrodynamics. In addition, the influences of thermal conductivity, velocity slip, Biot number and Nield boundary condition are also considered. An appropriate bvp4c along with 3-stage Lobatto IIIa method from MATLAB software is maneuvered to solve the two-

point boundary value problem using the similarity variables. The influences of several thermo physical parameters on velocity, temperature, nanoparticle spices concentration fields, skin friction, Nusselt number and Sherwood numbers are presented graphically and numerically. The results of the present study are compared with those of Wang [43], Gorla and Sidawi [44] and Khan and Pop [45] and found to be a good agreement.

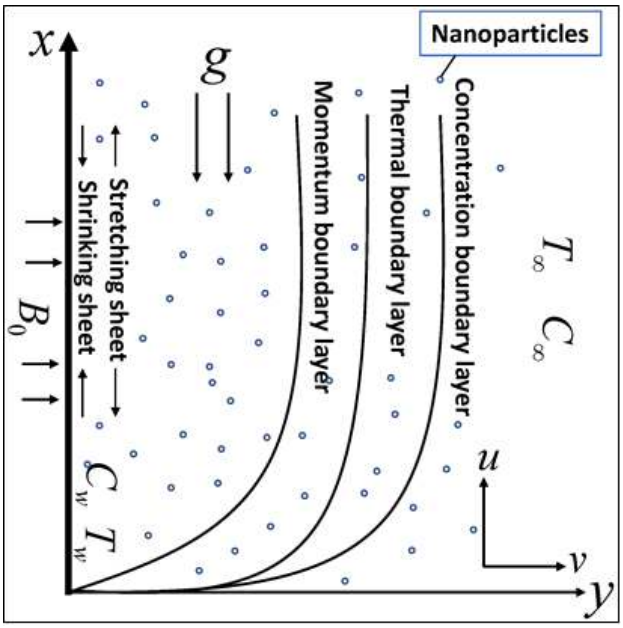

Figure 1: Schematic diagram of the physical model

2 Problem formulation

Let us assume a steady and incompressible thermally radiative MHD flow of Nanofluid induced by linear movement of stretching sheet embedded in fully saturated non-Darcy porous medium considering the influences of thermal conductivity, velocity slip, convective heat transfer and Nield boundary condition. The physical flow model and coordinate system is presented in Figure 1. The *x*-axis is considered along the stretching surface in the direction of the motion and *y*-axis is taken normal to the surface. The sheet is stretched along the x-axis with a velocity $u = U(x) = ax$, where a is a positive constant. The acceleration due to gravity, $\boldsymbol{g}$ is assumed to act downwards. A strong magnetic field having strength $\boldsymbol{B}_0$ is imposed in the normal direction. Both viscous and ohmic dissipation effects are neglected. By choosing a small Reynolds number, the aspects of the induced magnetic field are ignored.

Under these assumptions along with the Boussinesq and boundary layer approximations, the governing equations for Nanofluid [9–11] are:

$$\frac{\partial u}{\partial y} + \frac{\partial v}{\partial x} = 0 \tag{1}$$

$$u\frac{\partial u}{\partial x} + v\frac{\partial u}{\partial y} = \nu\frac{\partial^2 u}{\partial y^2} + g\left((1 - C_\infty)\rho_f\beta_T(T - T_\infty)\right.$$
$$\left. - (\rho_p - \rho_f)\beta_c(C - C_\infty)\right) - \frac{\sigma B_0^2}{\rho_f}u - \frac{\nu}{K^\star}u - \frac{C_b}{\sqrt{K^\star}}u^2 \tag{2}$$

$$u\frac{\partial T}{\partial x} + v\frac{\partial T}{\partial y} = \frac{k}{\rho c_p}\frac{\partial^2 T}{\partial y^2} - \frac{1}{\rho c_p}\frac{\partial q_r}{\partial y}$$
$$+ \frac{(\rho c)_p}{(\rho c)_f}\left(D_B\frac{\partial T}{\partial y}\frac{\partial C}{\partial y} + \frac{D_T}{T_\infty}\left(\frac{\partial T}{\partial y}\right)^2\right) \tag{3}$$

$$u\frac{\partial C}{\partial x} + v\frac{\partial C}{\partial y} = D_B\frac{\partial^2 C}{\partial y^2} + \frac{D_T}{T_\infty}\frac{\partial^2 T}{\partial y^2} - K_c(C - C_\infty)\left(\frac{T}{T_\infty}\right)^n e^{-\left(\frac{E_a}{kT}\right)} \tag{4}$$

Using Rosseland approximation, q_r can be expressed in non-linear form as:

$$q_r = -\frac{4\sigma^\star}{3k^\star}\frac{\partial T^4}{\partial y} \tag{5}$$

By assuming that the temperature differences within the flow are sufficiently small, using Taylor's series expansion, can be expressed as,

$$T^4 \cong 4T_\infty^3 T - 3T_\infty^4, \tag{6}$$

Using Eqs. (5) & (6) in (3), we get,

$$u\frac{\partial T}{\partial x} + v\frac{\partial T}{\partial y} = \frac{k}{\rho c_p}\frac{\partial^2 T}{\partial y^2} + \frac{16\sigma^\star T_\infty^3}{3k^\star \rho c_p}\frac{\partial^2 T}{\partial y^2}$$
$$+ \frac{(\rho c)_p}{(\rho c)_f}\left(D_B\frac{\partial T}{\partial y}\frac{\partial C}{\partial y} + \frac{D_T}{T_\infty}\left(\frac{\partial T}{\partial y}\right)^2\right) \tag{7}$$

The Navier's slip condition, convective condition and Nield boundary conditions are:

$$\begin{aligned} &u = U(x) + L\tfrac{\partial u}{\partial y}, \quad v = 0, \quad -k\tfrac{\partial T}{\partial y} = h_w(T_w - T), \\ &D_B\tfrac{\partial C}{\partial y} + D_T\tfrac{\partial T}{\partial y} = 0, \quad At \quad y = 0 \\ &u \to 0, \quad T \to T_\infty, \quad C \to C_\infty, \qquad As \quad y \to \infty \end{aligned} \tag{8}$$

Introducing the similarity variables:

$$\eta = \sqrt{\frac{a}{\nu}}y, \ \psi = \sqrt{a\nu}xf(\eta), \ \theta = \frac{T - T_\infty}{T_w - T_\infty}, \ \phi = \frac{C - C_\infty}{C_w - C_\infty} \tag{9}$$

The continuity equation is satisfied by considering the stream function $\psi(x, y)$ as follows:

$$u = \frac{\partial \psi}{\partial y}, \quad v = -\frac{\partial \psi}{\partial x}$$

Using Eq. (6) in Eqs. (2), (7) and (4), we get,

$$f''' + f f'' - (M + K_1) f' - (1 + Fr) \left(f'\right)^2 + \lambda (\theta - Nr\, \phi) = 0 \tag{10}$$

$$\frac{1}{\Pr} (1 + R)\, \theta'' + f\, \theta' + Nb\, \theta' \phi' + Nt \left(\theta'\right)^2 = 0 \tag{11}$$

$$\phi'' + Sc f\, \phi' + \frac{Nt}{Nb}\, \theta'' - Sc\, \sigma_R (1 + \delta\theta)^n \phi\, e^{-\left(\frac{E}{1+\delta\theta}\right)} = 0 \tag{12}$$

The prescribed two-point boundary conditions are redesigned as:

$$\begin{aligned} &f = 0, \quad f' = 1 + Sf'', \quad \theta = 1 + \tfrac{\theta'}{Bi}, \\ &Nt\, \theta' + Nb\, \phi' = 0 \quad at \quad \eta = 0 \\ &f' \to 0, \quad \theta \to 0, \quad \phi \to 0 \quad as \quad \eta \to \infty \end{aligned} \tag{13}$$

Where $K_c\,(C - C_\infty) \left(\frac{T}{T_\infty}\right)^n e^{-\left(\frac{E_a}{kT}\right)}$ is an Arrhenius expression, $Fr = \sqrt{\frac{\nu}{K^\star a}} C_b$, $K_1 = \frac{\nu}{aK^\star}$, $M = \frac{\sigma B_0^2}{a\rho_f}$, $\Pr = \frac{k}{\nu \rho c_p}$, $\lambda = \frac{(1-C_\infty) g \beta_T (T_w - T_\infty)}{x\, a^2}$, $Nr = \frac{(\rho_p - \rho_f)\beta_c (C_w - C_\infty)}{(1-C_\infty)\rho_f \beta_T (T_w - T_\infty)}$, $R = \frac{16\sigma^\star T_\infty^3}{3k\, k^\star}$, $S = L\sqrt{\frac{a}{\nu}}$, $Sc = \frac{\nu}{D_B}$, $Nb = \frac{D_B \tau (C_w - C_\infty)}{\nu}$, $Nt = \frac{D_T \tau (T_w - T_\infty)}{T_\infty \nu}$, $E = \frac{E_a}{k\, T_\infty}$, $Bi = \frac{h_w}{k}\sqrt{\frac{a}{\nu}}$, $\sigma_R = \frac{K_c}{a}$, $\delta = \frac{T_w - T_\infty}{T_\infty}$

To calculate the heat and concentration transfer rates, the physical quintiles shear stress rate (C_f), local Nusselt number (Nu_x) and local Sherwood number (Sh_x) are defined as:

$$C_f \mathrm{Re}_x^{1/2} = f''(0) \tag{14}$$

$$Nu_x\, \mathrm{Re}_x^{-1/2} = -(1 + R)\, \theta'(0) \tag{15}$$

$$Sh_x\, \mathrm{Re}_x^{-1/2} = -\phi'(0) \tag{16}$$

Here $\mathrm{Re}_x = \frac{ax^2}{\nu}$ is the local Reynolds number.

3 Numerical procedure

Mathematically, the system of coupled dimensionless Eqs. (7) – (9) subject to boundary conditions Eq. (10) is strongly non-linear and are indeed very difficult to solve analytically. Hence the bvp4c technique from matlab is used to solve this system of equations numerically.

The Matlab BVP solver bvp4c from matlab, a finite difference code which implements the 3stage Lobatto IIIa formula is used to obtain the numerical solutions. In this technique the Eqs. (7) - (9) are first transformed into a set of coupled first-order equations as follows:

$$y = \left[f\ f'\ f\ \ \theta\ \ \theta'\ \ \phi\ \ \phi'\right]^T \tag{17}$$

Therefore, Eqs. (7) – (8) can be written as:

$$\frac{d}{d\eta} \begin{bmatrix} y(1) \\ y(2) \\ y(3) \\ y(4) \\ y(5) \\ y(6) \\ y(7) \end{bmatrix} = \begin{bmatrix} y(2) \\ y(3) \\ -y(1)y(3) + (M + K_1)y(2) + (1 + Fr)\, y(2) * y(2) - \lambda \left(y(4) - Nry(6)\right) \\ y(5) \\ -\Pr \left(y(1)y(5) + Nby(5)y(7) + Nty(5)^2\right) / (1 + R) \\ y(7) \\ -Sc\, y(1)y(7) - \left(Nt/Nb\right)\, y'(5) + Sc\sigma \left(1 + \delta y(4)\right)^n y(6) \exp\left(-E/\left(1 + \delta\, y(4)\right)\right) \end{bmatrix} \tag{18}$$

And then this is set up as s boundary value problem (bvp) and use the bvp solver in matlab to solve the system along with the specified boundary conditions numerically using the RK method of order 4(i.e., bvp4c). The iterative process will be terminated when the error involved is $< 10^{-6}$.

For further information about the algorithm of bvp4c the readers can refer to Shampine *et al.* [46] and Ibrahim [47].

4 Results and discussion

The system of Eqs. (7) – (10) are solved using the bvp4c technique and the results of velocity, temperature, concentration, shear stress rate, Nusselt number and Sherwood number for distinct values of various dimensionless thermo-physical parameter namely, *Brownian motion parameter (Nb), thermophoresis parameter (Nt), buoyancy ratio parameter (Nr), Darcy number (K_1), Energy activation number (E*), *Forchheimer number (Fr), Velocity slip parameter (S), Biot number (Bi), magnetic parameter (M), radiation parameter (R), Prandtl number (Pr) and Schmidt number (Sc)* are presented graphically and numerically. The results of the present numerical code for reduced Nusselt number (local heat transfer rate, Nu_x) are compared with the solutions of Wang [43], Gorla & Sidawi [44] and Khan & Pop [45] for different values of *Pr* and are displayed in Table 1. Exceptionally excellent agreement is attained. To study the influence of the involved variables, other parameters are fixed as $Bi = 0.3$, $R = Nr = K_1 = Fr = S = \lambda = E = 0.1$, $Pr = 3$, $Sc = M = \sigma = 0.2$, $\delta = n = Nb = Nt = 0.5$. The results of shear stress rate (C_f), reduced local heat transfer coefficient (i.e., local Nusselt number, Nu_x) and reduced mass transfer coefficient (i.e., local Sherwood number, Sh_x) are presented in Table 2 for distinct values of *Pr*, *M*, *Nr*, *R*, λ, K_1, *E, Fr, Sc, S, Bi, Nb, and Nt*. A rise in *Pr* is noted to increase C_f, Nu_x and Sh_x. Hence the heat transfer to the surface is raised with lower thermal conductivity (higher Prandtl number) and the nanoparticle diffusion (mass transfer) is raised. Further, it is seen that C_f is enhanced with a rise n *M* values whereas both Nu_x and Sh_x are reduced. Fluid energizes with the impact of stronger magnetic field and the heat is expanded from the boundary that leads to further decrease in heat transfer to the wall. This process affects adversely on the nanoparticles diffusion to the wall. The magnetic quantities leads the energy to the fluid and improves the heat transportation through the sheet. Hence, the magnetic parameter could be used as a method for plotting the features of flow and heat transport. It is further seen that increasing *Nr* values reduces C_f, Nu_x and Sh_x since radiation stimulates the nanofluid. However, increment of *Nr* with high radiation implies elevation of nanoparticles diffusion to the boundary layer and diminishes nanoparticles concentration at the boundary layer. Also, an increase in radiation parameter is seen to decrease C_f and Sh_xbut Nu_x is boosted. Increasing mixed convection parameter (Richardson number) is seen to largely reduce C_f however, a significant rise is observed in the case of both Nu_x and Sh_x. An increase in Darcy number is seen to enhance C_f greatly but both Nu_x and Sh_x are seen to decrease. With a rise in activation energy number, a very slight variation is observed in C_f, Nu_x and Sh_x. A rise in velocity slip parameter is seen to reduce C_f, Nu_x and Sh_x. A rise in biot number is seen to enhance Nu_x and Sh_x. A rise in Schmidt number is seen to reduce Sh_x. A rise in Brownian motion parameter is seen to reduce Sh_x. A rise in Thermophoresis parameter is seen to enhance Sh_x.

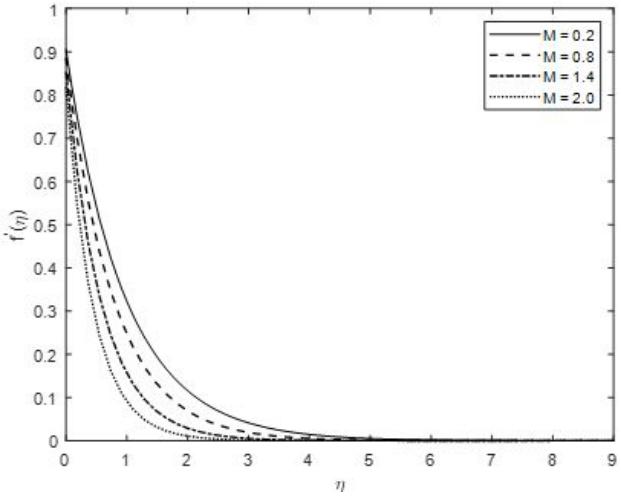

Figure 2: Variations of f′ for various *M* Values

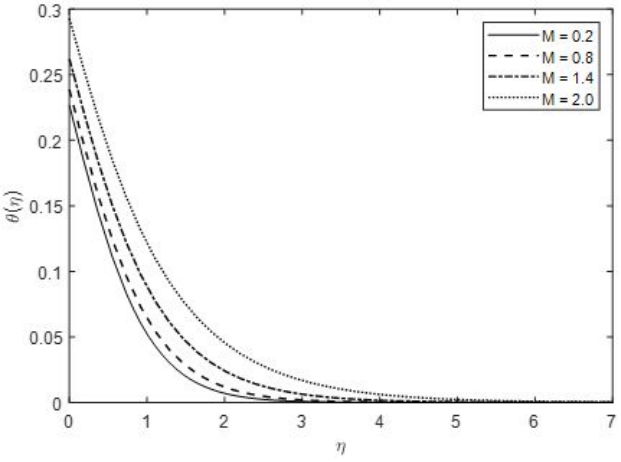

Figure 3: Variations of θ for various *M*

Figures 2 - 4 depicts the effect of *Hartmann number*, *M* on velocity, temperature and concentration distributions. A diminishing trend for velocity is noted as *M* increases. A strong Lorentz force substantially reduces the velocity with greater *M* values. As the Lorentz force is resistive, the velocity distribution decreases resulting in a reduction in particles motion. The temperature profiles are found

Table 1: Comparison values of Nu_x for various values of Pr.

Pr	Wang [43]	Gorla & Sidawi [44]	Khan & Pop [45]	Present
0.07	0.0656	0.0656	0.0663	0.0660
0.2	0.1691	0.1691	0.1691	0.1689
0.3	0.4539	0.5349	0.4539	0.4538
2	0.9114	0.9114	0.9113	0.9112
7	1.8954	1.8905	1.8954	1.8950
20	3.3539	3.3539	3.3539	3.3535
70	6.4622	6.4622	6.4621	6.4620

Table 2: Values of C_f, Nu_x and Sh_x

Pr	M	Nr	R	λ	K_1	E	Fr	Sc	S	Bi	Nb	Nt	C_f	Nu_x	Sh_x
3	0.2	0.1	0.1	0.1	0.1	0.1	0.1	0.2	0.1	0.3	0.5	0.5	0.9424	0.2552	0.2320
4													0.9442	0.2648	0.2407
5													0.9453	0.2714	0.2467
6													0.9461	0.2763	0.2512
	0.5												1.0172	0.2538	0.2307
	1.0												1.2394	0.2490	0.2264
	1.5												1.5196	0.2420	0.2200
	2.0												1.8150	0.2333	0.2121
		1											0.9411	0.2552	0.2320
		5											0.9366	0.2549	0.2317
		7											0.9357	0.2547	0.2315
			0.5										0.9398	0.3321	0.2214
			1.0										0.9368	0.4205	0.2103
			1.5										0.9340	0.5020	0.2008
				1									0.8731	0.2562	0.2329
				5									0.6038	0.2594	0.2359
				10									0.3191	0.2621	0.2383
				15									0.0686	0.2640	0.2400
					1.0								1.2235	0.2494	0.2267
					2.0								1.4573	0.2436	0.2215
					3.0								1.6460	0.2384	0.2167
						0.5							0.9424	0.2553	0.2320
						1.5							0.9425	0.2553	0.2321
						3.0							0.9425	0.2553	0.2321
							5.0						1.6126	0.2445	0.2222
							10						1.9917	0.2372	0.2156
							15						2.2622	0.2314	0.2104
									0.5				0.6280	0.2466	0.2242
									1.0				0.4518	0.2392	0.2175
									1.5				0.3556	0.2337	0.2124
										0.5				0.3694	0.3358
										0.8				0.4933	0.4485
										1.2				0.6062	0.5511
								0.5							0.2317
								1.0							0.2312
								1.5							0.2308
											0.1				1.1600
											0.2				0.5800
											0.3				0.3867
												0.1			0.0465
												0.2			0.0929
												0.3			0.1393

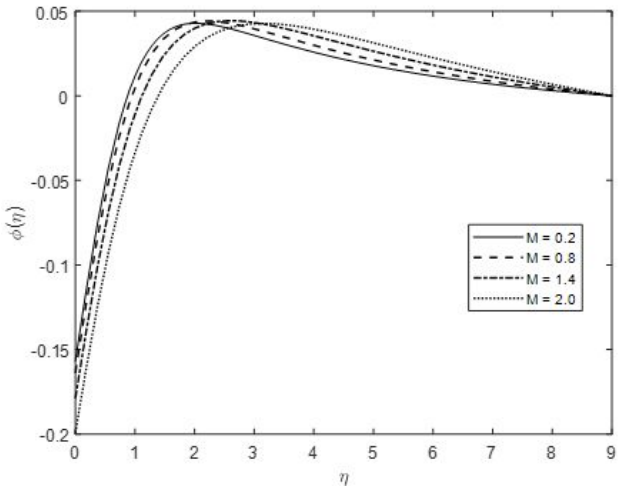

Figure 4: Variations of ϕ for various M

to increase as M increases. The greater variance in M includes Lorentz forces resisting the motion of the fluid particles and increases the temperature profiles. When the fluid flow decreases the energy is released as heat, resulting in a thickening of the thermal boundary layer. A slight decrease in the concentration profiles is observed with a rise in M values.

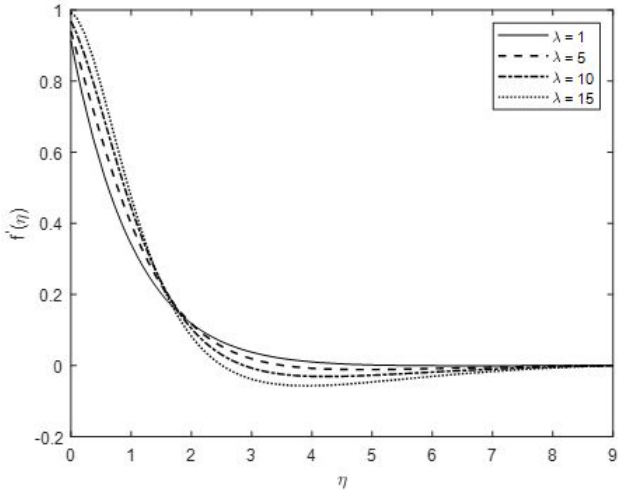

Figure 5: Variations of f′ for various λ

Figures 5 - 7 display the effects of *Richardson number*, λ on the velocity, temperature and concentration distributions. The velocity increases with a rise in λ values. Physically, the mixed convection parameter compares buoyancy and viscous forces. The viscous forces are reduced when the mixed convection parameter is increased, which improves the velocity shift. A very slight decrease in tempera-

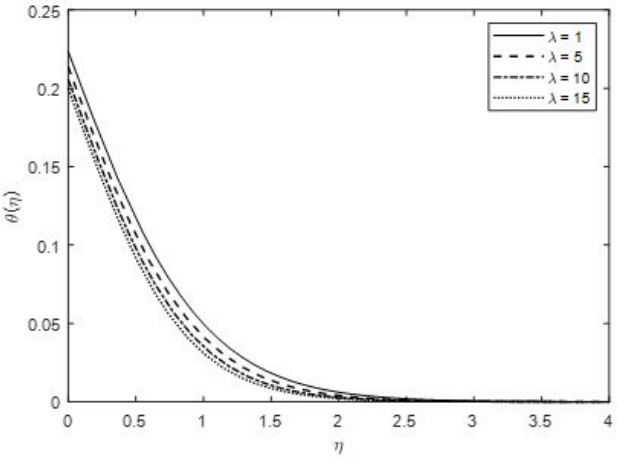

Figure 6: Variations of θ for various λ

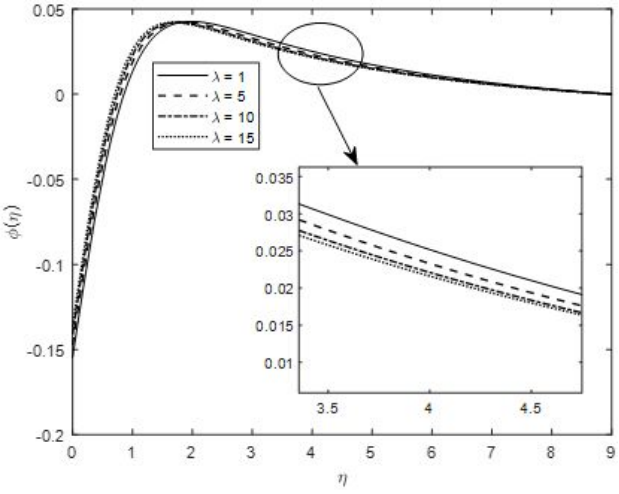

Figure 7: Variations of ϕ for various λ

ture is noted with a rise in λ values. The fluid density varies with temperature variation due to thermal expandability and the flow can be influenced by the buoyancy force. As a consequence, the more we go from pure force convection ($\lambda = 0$) to natural convection under defined Reynolds, the more cooler the interface becomes. The nanoparticle concentration is noted to increase with an increase in λ.

Figures 8 – 10 display the effect of *Darcy number*, K_1, on the velocity, temperature and concentration distributions. An increase in K_1 values leads the velocity profiles to decay. The existence of permeable space increases the fluid stream safety by lowering fluid velocity and the energy layer associated with it. Physically, the presence of porosity causes resistance to fluid motion, resulting in a reduction in fluid velocity. The temperature profiles are enhanced with a rise in K_1 values. Porousness, in general, increases fluid flow resistance, resulting in increased tem-

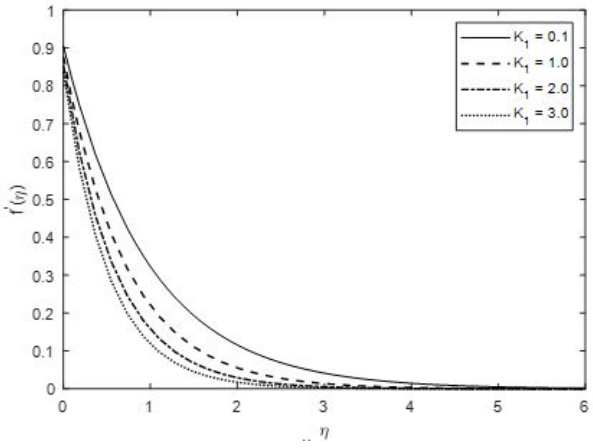

Figure 8: Variations of f′ for various K_1

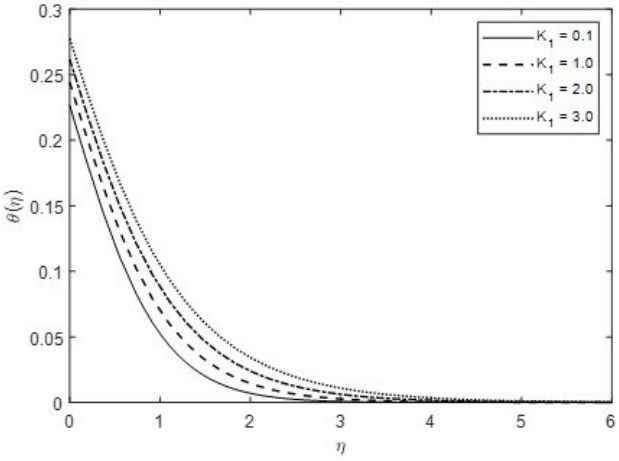

Figure 9: Variations of θ for various K_1

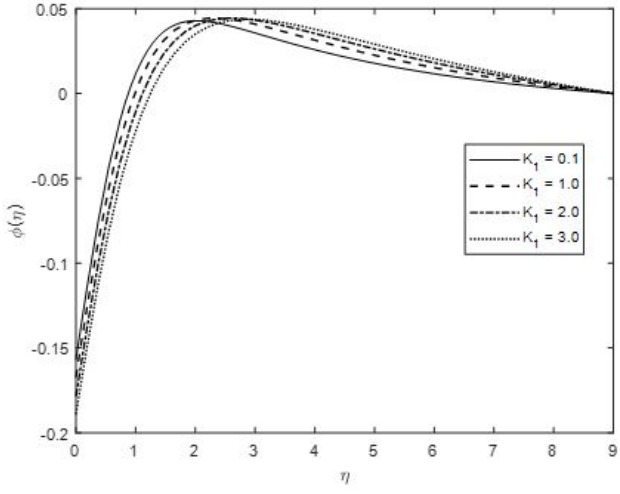

Figure 10: Variations of ϕ for various K_1

perature profiles and thermal boundary layer thickness. The concentration profiles are seen to decrease with a rise in K_1 values. It is noted that the presence of porous media increases the flow resistance, resulting in improved temperature distribution.

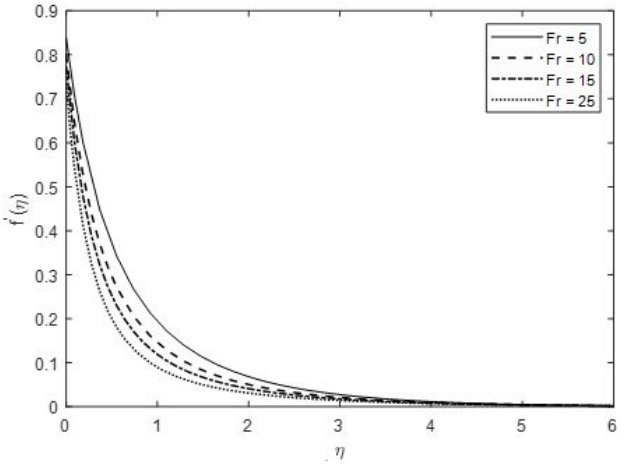

Figure 11: Variations of f′ for various Fr

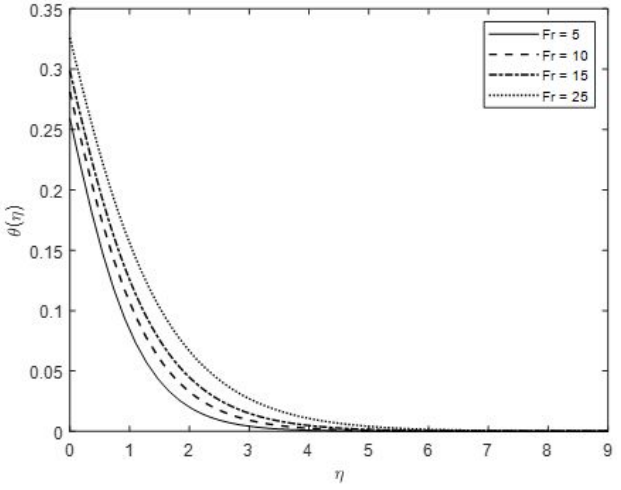

Figure 12: Variations of θ for various Fr

Figures 11 – 13 portrays the effect of *Forchheimer parameter*, *Fr*, on the velocity, temperature and concentration distributions. The velocity profiles are lowered with greater values of *Fr* since the inertia coefficient is directly proportional to the drag coefficient. Therefore, the drag coefficient increases as *Fr* increases. As a consequence, the fluid's resistance force increases and hence the velocity decreases. An increase in *Fr* values leads to thickening the thermal boundary layer and doesn't allow the fluid to pass easily. The temperature profiles are strongly in-

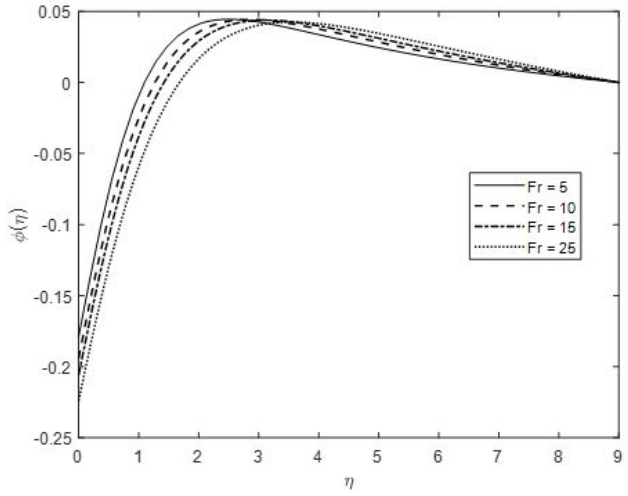

Figure 13: Variations of ϕ for various Fr

creased with the raising values of Fr. However, the concentration profiles are lowered with increasing Fr values.

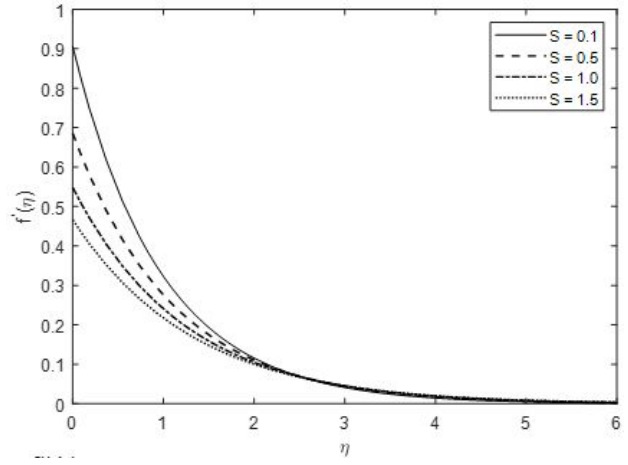

Figure 14: Variations of f′ for various S

Figures 14 - 16 display the effect of *velocity slip parameter, S*, on the velocity, temperature and concentration distributions. A decay in velocity profile is seen with an increase in S values. As the S values raise, the stretching impacts are partly pass through the fluid and hence the velocity decreases. An increase in S values is noted to increase both temperature and concentration profiles. If $S = 0$, the fluid holds to the boundary and the fluid slides with no resistance as $S \to \infty$. As the S values increase, the motion of the fluid particles declines and hence the temperature and concentration increases.

Figures 17 - 18 display the effect of *Prandtl number, Pr* on the temperature and concentration distributions. Generally, the temperature profiles decline with a rise in Pr

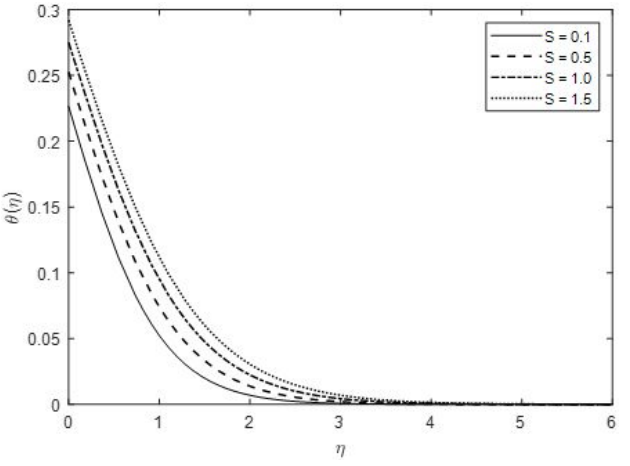

Figure 15: Variations of θ for various S

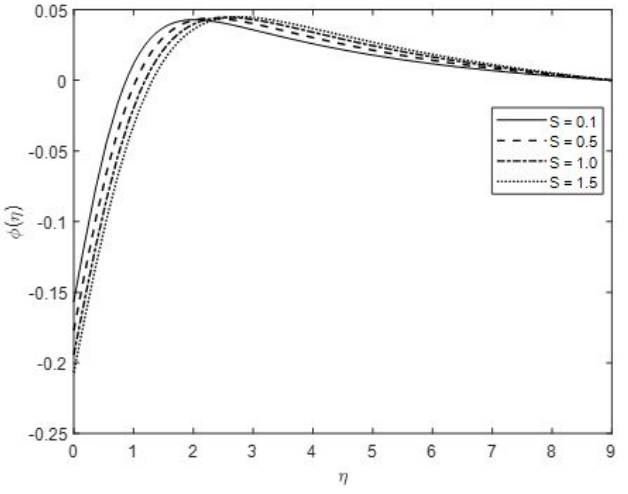

Figure 16: Variations of ϕ for various S

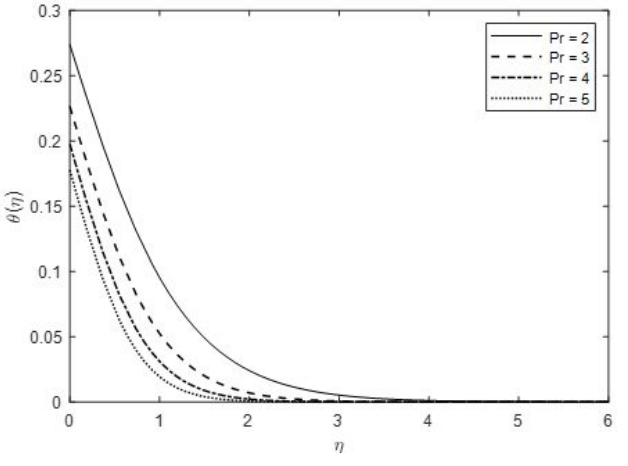

Figure 17: Variations of θ for various Pr

values. The parameter Pr plays a significant role in engineering and manufacturing processes. The Prandtl num-

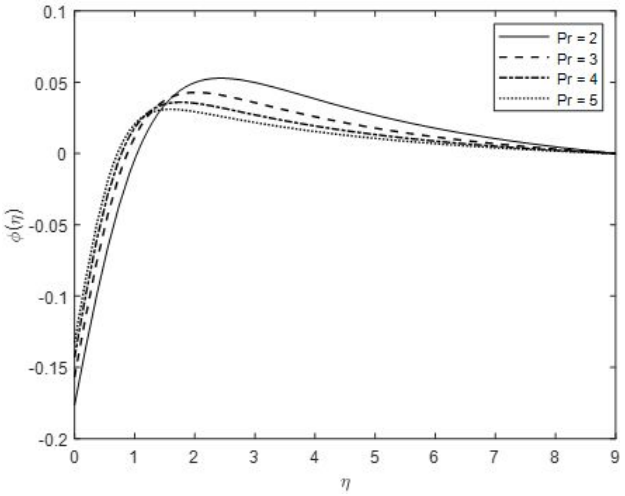

Figure 18: Variations of ϕ for various Pr

ber is defines as the ratio of force diffusivity to warm diffusivity. Clearly, Pr is inversely related to thermal diffusivity. Hence for greater Pr values the thermal diffusivity is very low. High values of *Pr* lead the fluid become more viscous and small values of *Pr* lead the fluid become less viscous. Therefore, increasing *Pr* causes the fluid temperature to decrease. A significant reduction in concentration profiles is observed with a rise in *Pr* values.

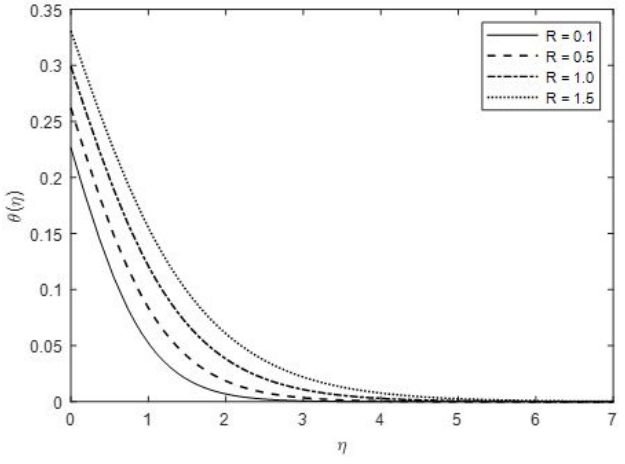

Figure 19: Variations of θ for various R

Figure 19 - 20 display the effect of *thermal radiation*, *R*, on the temperature and concentration distributions. A strong elevation in temperature and concentration profiles is noted with a rise in *R* values. This is due to the fact that certain amount of heat energy is emitted during the radiation cycle.

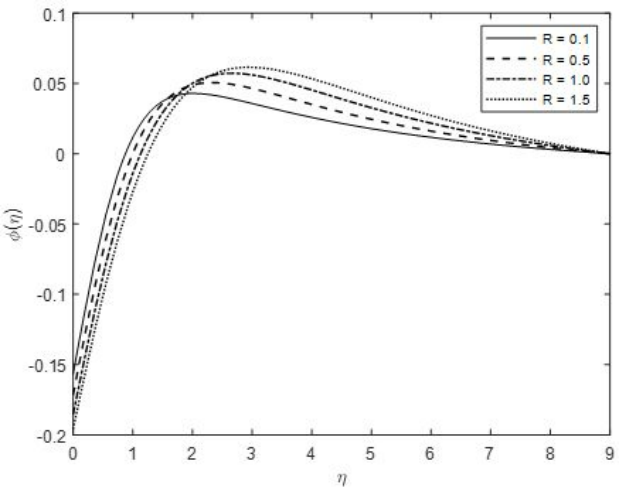

Figure 20: Variations of ϕ for various R

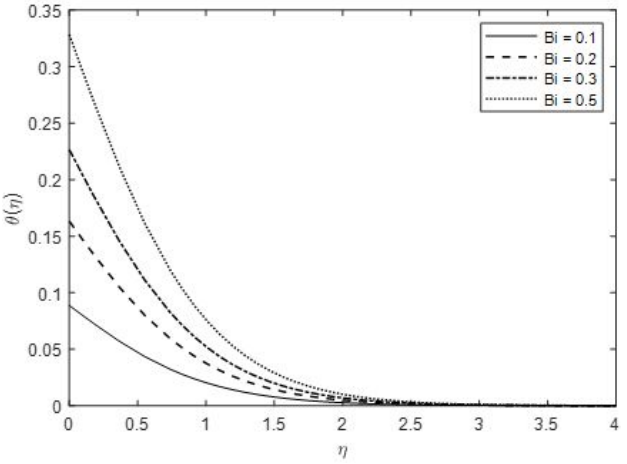

Figure 21: Variations of θ for various Bi

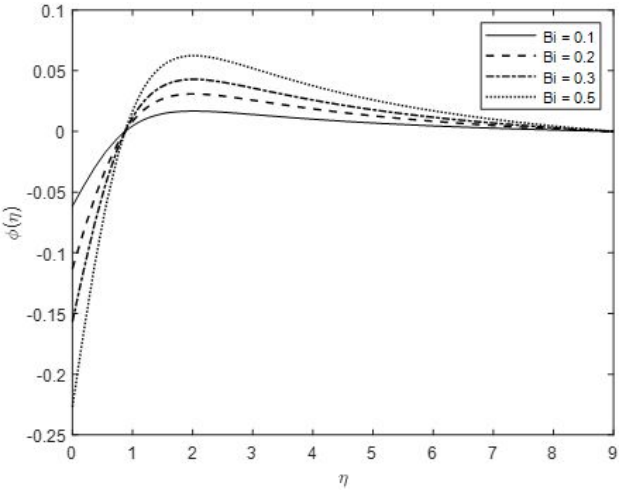

Figure 22: Variations of ϕ for various Bi

Figures 21 – 22 display the effect of *Biot number, Bi* on the temperature and concentration distributions. A strong increase in both temperature and concentration profiles is seen with a rise in *Bi* values. The buoyancy force increases as the Biot number rises and the fluid carries the heat energy at a faster rate. Due to thermal expandability, the fluid density varies with temperature and the flow is influenced by the buoyancy force. Biot number is defined as the relationship between solid conduction and surface convection. Physically, as the Biot number rises, the surface's thermal resistance decreases dramatically. Convection is increased, resulting in a higher surface temperature.

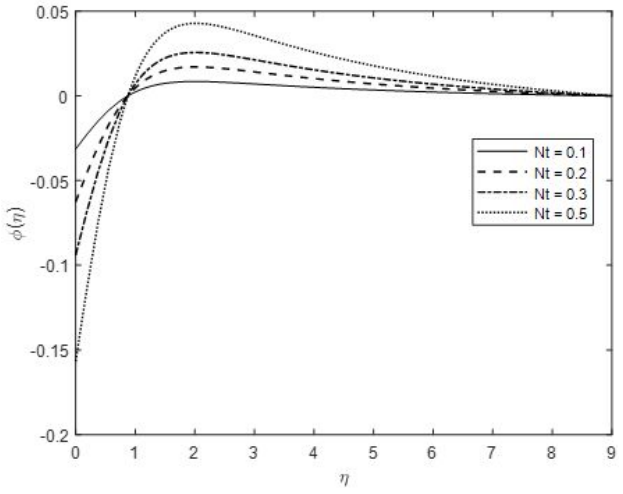

Figure 23: Variations of ϕ for various Nt

Figure 23 display the effect of *thermophoresis parameter, Nt*, on the concentration distributions. The process of moving the particles so that they contract temperature due to the temperature gradient force is called thermophoresis. The parameter *Nt*, plays a crucial role in nanoparticle volume fraction. A significant enhancement is observed in the concentration profile with an increase in *Nt* values. As *Nt* increases, the heat transfer in the boundary layer rises and at the same time exacerbates particle deposition away from the fluid region, thereby raising the nanoparticles volume fraction.

Figure 24 display the effect of *Brownian motion parameter, Nb,* on the concentration distributions. The nanoparticle concentration is substantially decreased with increasing *Nb* vales. The nanoparticles reorganize to create a new structure because of the spontaneous diffusivity. Thus the thermal conductivity of the nanofluid is improved. The Brownian motion warms the fluid in the boundary layer

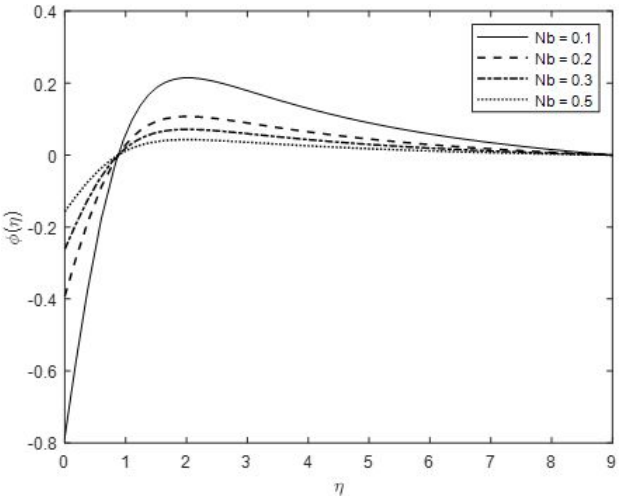

Figure 24: Variations of ϕ for various Nb

and rages the particles away from the fluid system thereby reducing the concentration distributions.

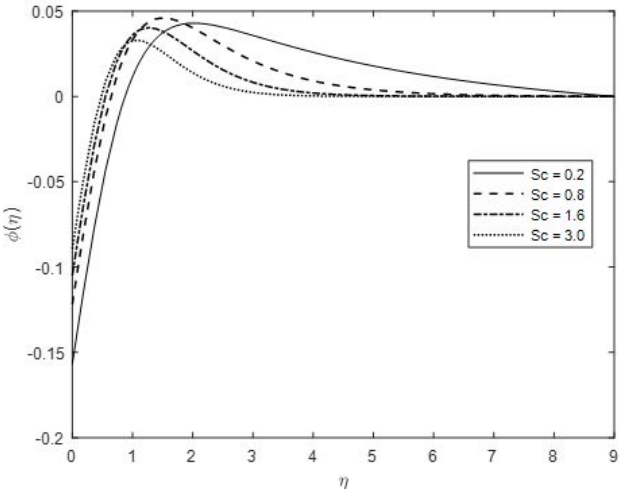

Figure 25: Variations of ϕ for various Sc

Figure 25 display the effect of *Schmidt number*, *Sc*, on the concentration distributions. A significant decrease in concentration profiles and the corresponding boundary layer thickness is noted with a rise *Sc* values. By def., *Sc* represents the diffusion ratio of momentum to mass. Hence, mass diffusivity is the reason for the decrease in the concentration.

Figure 26 display the effect of *Reaction rate*, σ_R, on the concentration distributions. A significant reduction in concentration profiles is noted with rising σ values. An increase in σ values results in an increase in the Arrhenius expression which eventually damages the chemical reaction. Hence the concentration profiles decay.

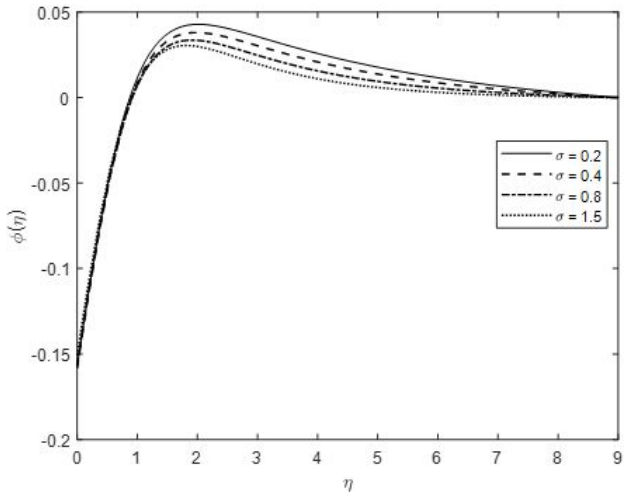

Figure 26: Variations of ϕ for various σ

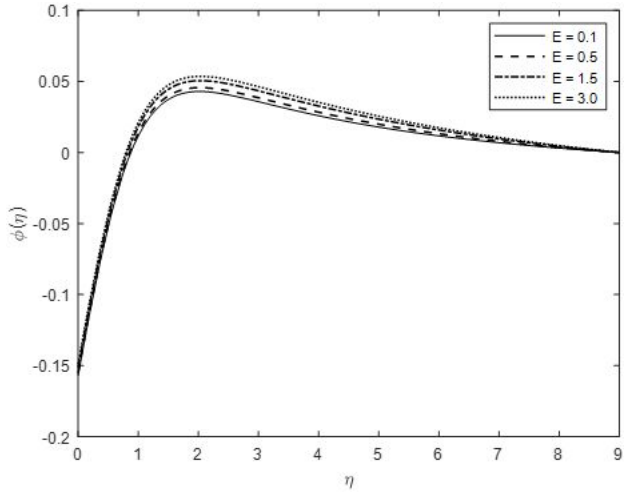

Figure 27: Variations of ϕ for various E

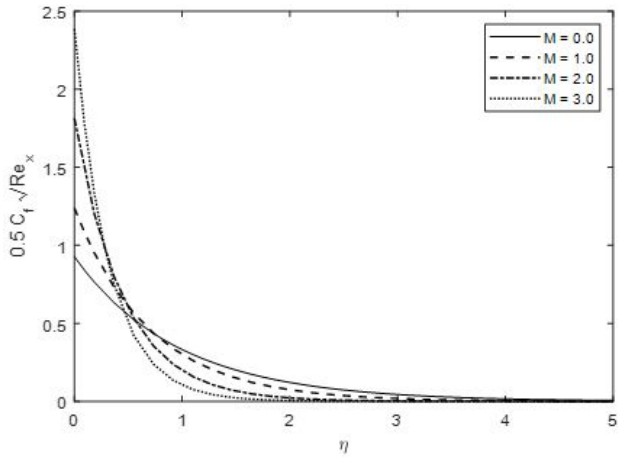

Figure 28: Variations of Cf_x for various M values

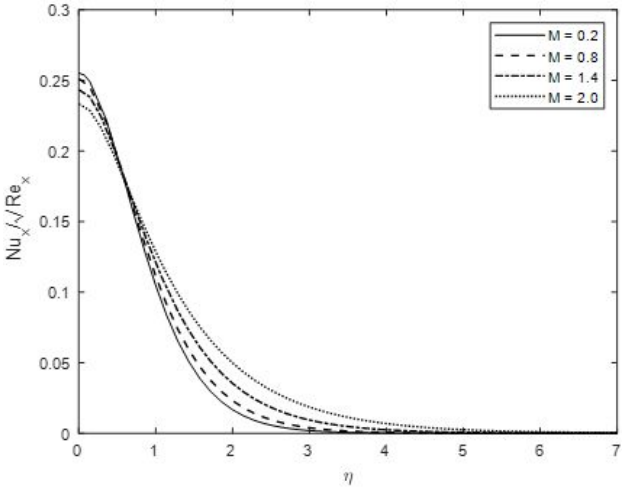

Figure 29: Variations of Nu_x for various M values

Figure 27 illustrates the influence of *Energy activation number*, E, on the concentration profiles. It is found that the concentration profiles increase with an increase in E values. Usage of activation energy is more efficient in enhancing the reaction process and hence increasing the concentration. The Arrhenius expression declines with an increase in E values, resulting in the development of the relational chemical reaction leading to an increase in the concentration profiles. Due to the phenomenon of low temperature and greater activation energy results in a lower reaction rate that slows down the chemical reaction. This way the concentration increases.

Figures 28 – 29 depicts the influences of magnetic parameter M on skin friction and heat transfer rate. It has been seen that as the values of M increases, the skin friction increases near the wall and as we move away from the wall it decreases and a quite opposite trend is observed in the case of heat transfer rate. This confirms the earlier observations that the flow is slowed by the magnetic field but the fluid is heated. Higher heat transfer rates and a decrease in fluid temperature are associated with heat transfer from the fluid to the surface.

Figures 30 – 31 depicts the influences of radiation parameter R on heat and mass transfer rates. A greater increase in heat transfer rate is observed with a rise in radiation parameter whereas the mass transfer rate is decreased. The flow is accelerated by the strong radiation, but the heat transfer to the surface is reduced. Species diffusion to the surface is hampered by the greater contribution of thermal conduction heat transfer.

Figure 32 – 33 depicts the influences of velocity slip S and Darcy number K_1 on skin friction. A significant decrease in skin friction is seen with an increase in velocity slip. With an increase in Darcy number the skin friction is

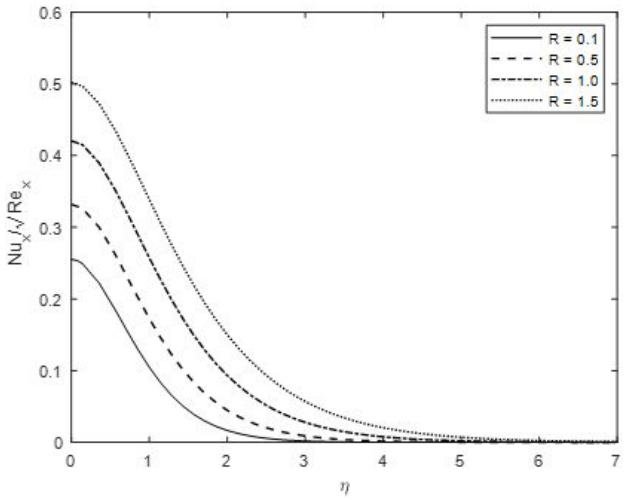

Figure 30: Variations of Nu_x for various R values

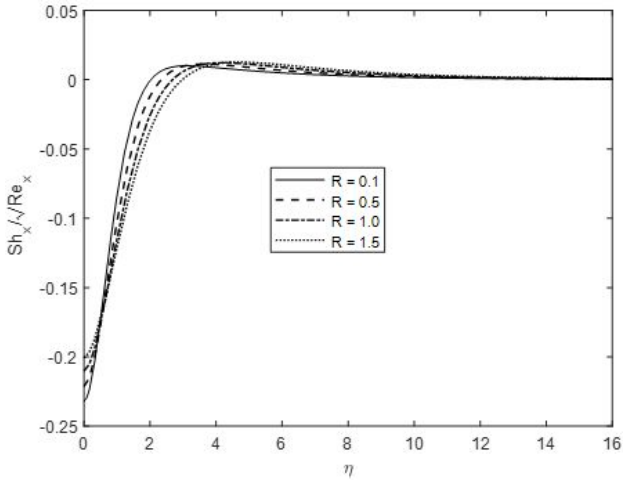

Figure 31: Variations of Sh_x for various R values

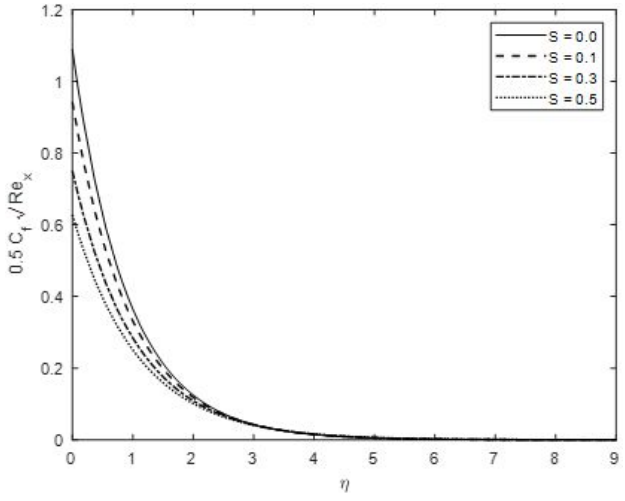

Figure 32: Variations of Cf_x for various S values

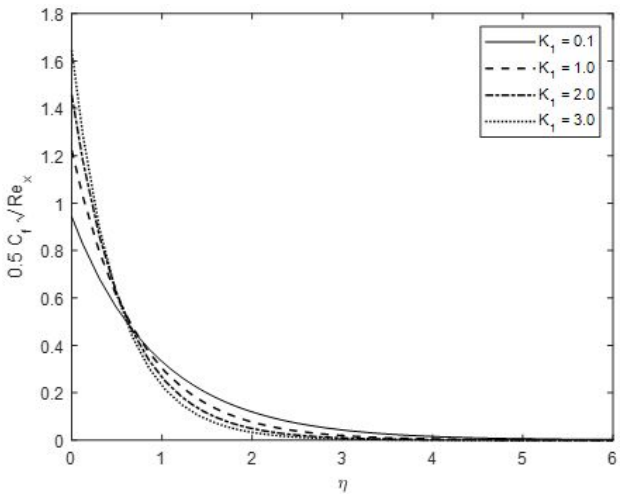

Figure 33: Variations of Cf_x for various K_1 values

increased slightly near to the wall and as we move away from the wall the skin friction is decreased.

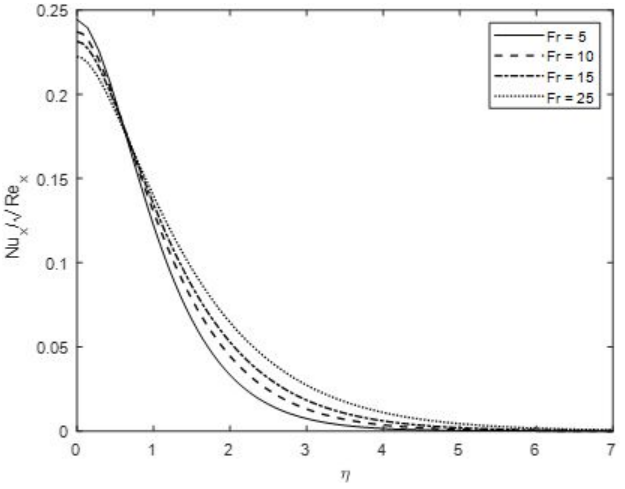

Figure 34: Variations of Nu_x for various Fr values

Figure 34 presents the influences of Forchheimer number *Fr* on heat transfer rate. With an increase in *Fr*, the skin friction is slightly decreased near the wall and as we move away from the wall it is increased significantly.

Figure 35 illustrates the influences of Schmidt number *Sc* and *reaction rate*, σ_R on mass transfer rate. The mass transfer rate is increased with an increase in *Sc* values. While the mass transfer rate is decreased with an increase in σ_R values. An increase in *Sc* results in a decline in species mass diffusivity and hence increases mass transfer rate.

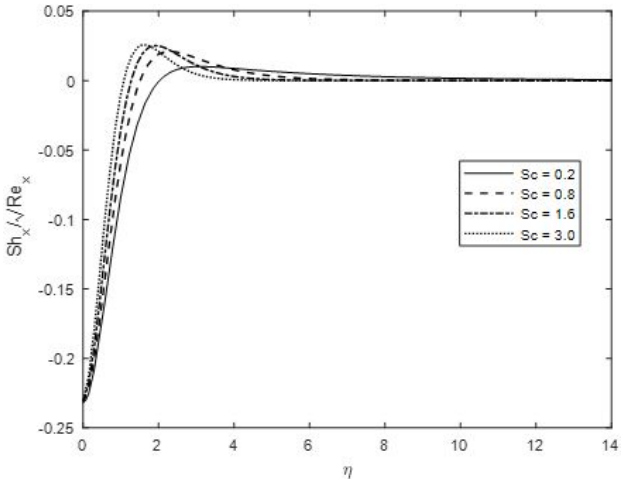

Figure 35: Variations of Sh_x for various Sc values

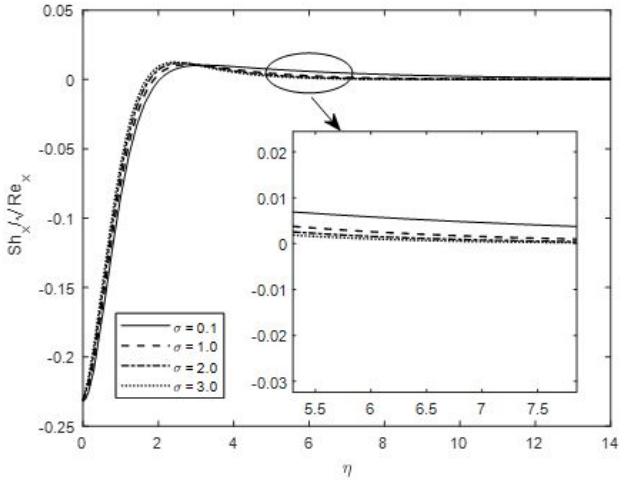

Figure 36: Variations of Sh_x for various σ values

5 Conclusion

The present analytical study focuses on the thermally radiative electrically conducting Darcy-Forchheimer Nanofluid flow characteristics past a stretching sheet considering the effects of thermal conductivity, velocity slip, convective heat transfer and Arrhenius activation energy. The governing flow equations are converted into ordinary differential equations (ODE's) with appropriate similarity transformations. Bvp4c technique is utilized in order to obtain the results. The present numerical code is validated with the previous results available in literature. The influences of various flow controlled parameters on velocity, temperature and nanoparticle volume fraction as well as shear stress rate, local Sherwood and Nusselt numbers presented and numerically and graphically. The observations of as follows:

1. The fluid velocity is decreased with increasing values of M whereas the fluid temperature and concentration are increased.
2. Increasing mixed convection parameter elevates the fluid velocity and nanoparticle concentration slightly whereas temperature is slightly increased.
3. Increasing Darcy number is noted to reduce the fluid velocity and nanoparticle concentration whereas temperature is enhanced. A similar behavior is observed with an increase in Forchheimer number and velocity slip parameter.
4. Increasing Pr reduces the temperature and nanoparticles concentration. Conversely, increasing Biot number enhances both temperature and nanoparticles concentration.
5. Increasing radiation parameter enhances the fluid temperature and nanoparticle concentration.
6. Increasing thermophoresis parameter strongly accelerates the nanoparticle concentration whereas increasing Brownian motion parameter and Schmidt number reduces nanoparticle concentration.
7. The nanoparticles concentration is decreased with increasing reaction rate parameter whereas increased slightly with increasing activation energy parameter.

Nomenclature:

a	Positive constant associated with linear stretching
Bi	Thermal Biot number
B_0	Constant imposed magnetic field
C	Concentration of the fluid
C_b	Forchheimer inertial Drag coefficient
c_p	Specific heat parameter
D_T	Thermophoretic diffusion constraint.
D_B	Brownian diffusivity
E_a	Activation energy
E	Energy activation number
f	Non-dimensional steam function
Fr	Inertia-coefficient (Forchheimer number)
g	Acceleration due to gravity
h_w	Convective heat transfer coefficient
k^*	Rosseland's mean absorption coefficient
k	Thermal conductivity
K^*	Permeability
K_1	Darcy parameter
K_c	Reaction rate
L	The parameter related to velocity slip
n	motile density
M	Hartmann number
Nr	Buoyancy parameter

Nb	Brownian motion Constraint
Nt	Thermophoresis parameter
Pr	Prandtl number
q_r	Radiative heat flux
R	Radiation parameter
S	Velocity slip parameter
Sc	Schmidt number
T	Temperature of Nanofluid
T_w	convective fluid temperature
u, v	The velocity components along (x, y) directions

Greek symbols

β_T	Thermal expansion coefficient
β_c	Concentration expansion coefficient
λ	The buoyancy or mixed convective parameter
ρ_f	Base fluid density
$(\rho c)_p$	Effective nano particles heat capacity
ρ_p	Nanoparticle density
ν	Kinematics viscosity
σ	Electric conductivity of the fluid
$(\rho c)_f$	Fluid heat capacity
α_f	Thermal diffusivity
σ_R	Reaction rate constant
δ	Temperature difference parameter
σ^*	Stefan-Boltzmann constant
θ	Non-dimensional temperature
φ	Non-dimensional concentration
ψ	Dimensionless stream function
η	The dimensionless radial coordinate
μ	Dynamic viscosity

Subscripts

∞	Free stream condition
w	wall condition

Funding information: The authors state no funding involved.

Author contributions: All authors have accepted responsibility for the entire content of this manuscript and approved its submission.

Conflict of interest: The authors state no conflict of interest.

References

[1] Buongiorno J. Convective transport of nanofluids. J Heat Transfer. 2006;128(3):240–50.
[2] Ellahi R, Zeeshan A, Shehzad N, Alamri SZ. Structural Impact of Kerosene-Al_2O_3 Nanoliquid on MHD Poiseuille Flow with Variable Thermal Conductivity: Application of Cooling Process. J Mol Liq. 2018;264:607–15.
[3] Choi SU. Enhancing thermal conductivity of fluids with nanoparticles, Developments and applications of non-Newtonian flows. Siginer DA, Wang HP (Eds.). FED-The American Society of Mechanical Engineers. 1995;231/MD(66):99-105.
[4] Patil PM, Shashikant A, Momoniat E. Transport phenomena in MHD mixed convective nanofluid flow. Int J Numer Methods Heat Fluid Flow. 2020;30(2):769–91.
[5] Khan NS, Shah Q, Bhaumik A, Kumam P, Thounthong P, Amiri I. Entropy generation in bioconvection nanofluid flow between two stretchable rotating disks. Sci Rep. 2020 Mar;10(1):4448.
[6] Nainaru Tarakaramu PV. Satya Narayana and Bhumarapu Venkateswarlu, Numerical simulation of variable thermal conductivity on 3D flow of nanofluid over a stretching sheet. Nonlinear Eng. 2020;9(1):233–43.
[7] Shiriny A, Bayareh M, Ahmadi Nadooshan A. Nanofluid flow in a microchannel with inclined cross-flow injection. SN Appl. Sci. 2019;1(9):1015.
[8] Suhail Ahmad Khan D, Altamush Siddiqui M. Numerical studies on heat and fluid flow of nanofluid in a partially heated vertical annulus. Heat Transfer. 2020;49(3):1458–90.
[9] Abdul Gaffar S, Ramachandra Prasad V, Rushi B, Anwar Beg O. Computational solutions for mixed convection boundary layer flows of Nanofluid from a non-isothermal wedge. J Nanofluids. 2018;7(5):1024–32.
[10] Abdul Gaffar S, Ramachandra Prasad V, Ramesh Reddy P. Hidayathulla Khan, Venkatadri K, Magnetohydrodynamic Non-Darcy Flows of Nanofluid from Horizontal circular permeable cylinder: A Buongiorno's mathematical model. J Nanofluids. 2019;8(2):276–86.
[11] Ghasemi SE, Hatami M. Solar radiation effects on MHD stagnation point flow and heat transfer of a nanofluid over a stretching sheet. Case Stud Therm Eng. 2021;25:100898.
[12] Alfvén H. Existence of electromagnetic-hydrodynamic waves. Nature. 1942;150(3805):405–6.
[13] Sing K, Pandey AK, Kumar M. Melting heat transfer assessment on magnetic nanofluid flow past a porous stretching cylinder. J Egypt Math Soc. 2021;29(1):1.
[14] Basant K. Jha, Peter B. Malgwi, Hall and ion-slip effects on MHD mixed convection flow in a vertical microchannel with asymmetric wall heating. Engineering Reports. 2020;2(9):e12241.
[15] Mohidul Haque M. Heat and Mass Transfer Analysis on Magneto Micropolar Fluid Flow with Heat Absorption in Induced Magnetic Field. Fluids. 2021;6(3):126.
[16] Alam J, Murtaza G, Tzirtzilakis E, Ferdows M. Jahangir Alam, Ghulam Murtaza, Efstratios Tzirtzilakis and Mohammad Ferdows, Biomagnetic Fluid Flow and Heat Transfer Study of Blood with Gold Nanoparticles over a Stretching Sheet in the Presence of Magnetic Dipole. Fluids. 2021;6(3):113.
[17] Md B. Hidayathulla Khan, S. Abdul Gaffar, Khalil-Ur-Rehman &

O. Anwar Beg, Entropy generation in magnetohydrodynamic radiative non-Newtonian Dissipative convection flow From an inclined plane: Numerical study, *Nanoscience and Technology*. Int J. 2020;11(4):297–326.
[18] Vedavathi N, Dharmaiah G, Abdul Gaffar S, Venkatadri K. Entropy analysis of magnetohydrodynamic nanofluid transport from an inverted cone: Buongiorno's model. Heat Transfer Journal; 2020. https://doi.org/10.1002/htj.22021.
[19] Khan M, Rasheed A, Salahuddin T. Radiation and chemical reactive impact on tangent hyperbolic fluid flow having double stratification. AIP Adv. 2020;10(7):075211.
[20] Tunde A. Yusuf, Fazle Mabood, B. C. Prasannakumara and Ioannis E. Sarris, Magneto-Bioconvection Flow of Williamson Nanofluid over an Inclined Plate with Gyrotactic Microorganisms and Entropy Generation. Fluids. 2021;6(3):109.
[21] Jawad M, Saeed A, Tassaddiq A, Khan A, Gul T, Kumam P, et al. Insight into the dynamics of second grade hybrid radiative nanofluid flow within the boundary layer subject to Lorentz force. Sci Rep. 2021 Mar;11(1):4894.
[22] Ge-JiLe H, Nazeer M, Hussain F, Khan MI, Saleem A, Siddique I. Hu Ge-JiLe, Mubbashar Nazeer, Farooq Hussain, M Ijaz Khan, Adila Saleem and Imran Siddique, Two-phase flow of MHD Jeffrey fluid with the suspension of tiny metallic particles incorporated with viscous dissipation and Porous Medium. Adv Mech Eng. 2021;13(3):1–15.
[23] Jawad M, Saeed A, Khan A, Ali I, Alrabaiah H, Gul T, et al. Analytical study of MHD mixed convection flow for Maxwell nanofluid with variable thermal conductivity and Soret and Dufour effects. AIP Adv. 2021;11(3):035215.
[24] Darcy H. Les Fontaines Publiques De La Ville De Dijon. Paris: Victor Dalmont; 1856.
[25] Forchheimer P. Wasserbewegung durch boden. Z Ver D Ing. 1901;45:1782–8.
[26] Pop I, Ingham DB. Mathematical and Computational Modeling of Viscous Fluids and Porous Media. Convective Heat Transfer. Oxford: Pergamon; 2001.
[27] Vafai K. Handbook of Porous Media. 2nd ed. New York: Taylor and Francis Group; 2005. https://doi.org/10.1201/9780415876384.
[28] Hayat T, Aziz A, Muhammad T, Alsaedi A. Effects of binary chemical reaction and Arrhenius activation energy in Darcy–Forchheimer three-dimensional flow of nanofluid subject to rotating frame. J Therm Anal Calorim. 2019;136(4):1769–79.
[29] Mir Asma WA. Othman, Taseer Muhammad, Numerical Study for Darcy-Forchheimer flow of Nanofluid due to a Rotating Disk with Binary Chemical Reaction and Arrhenius Activation Energy. Mathematics. 2019;7(10):921.
[30] Muhammad Ramzan, Nomana Abid, Dianchen Lu and Iskander Tlili, Impact of melting heat transfer in the timedependent squeezing nanofluid flow containing carbon nanotubes in a Darcy-Forchheimer porous media with Cattaneo-Christov heat flux, Commun. Theor. Phys. 2020;72:085801(11pp) https://doi.org/10.1088/1572-9494/ab8a2c..
[31] Ahmad S, Ali K, Rizwan M, Ashraf M. Heat and Mass Transfer Attributes of Copper-Aluminum Oxide Hybrid Nanoparticles Flow through a Porous Medium. Case Stud Therm Eng. 2021;25:100932.
[32] Rabiha S. Kareem, and Ahmed M. Abdulhadi, A study of MHD and Darcy-Forchheimer effects on third grade flow with Cattaneo-Christov heat flux. AIP Conf Proc. 2020;2292:020001.
[33] Jawad M. Anwar Saeed, Aurungzeb Khan, Saeed Islam, MHD bioconvection Darcy-Forchheimer flow of Casson nanofluid over a rotating disk with entropy optimization. Heat Transfer; 2020. pp. 1–29.
[34] Zhang L, Bhatti MM, Michaelides EE. Electro-magnetohydrodynamic flow and heat transfer of a third-grade fluid using a Darcy-Brinkman-Forchheimer model. Int J Numer Methods Heat Fluid Flow. 2020;ahead-of-print ahead-of-print: https://doi.org/10.1108/HFF-09-2020-0566.
[35] Khan U, Zaib A, Baleanu D, Sheikholeslami M, Wakif A. Exploration of dual solutions for an enhanced cross liquid flow past a moving wedge under the significant impacts of activation energy and chemical reaction. Heliyon. 2020 Jul;6(7):e04565.
[36] Aldabesh A, Ullah Khan S, Habib D, Waqas H, Tlili I, Ijaz Khan M, et al. Sami Ullah Khan, Danial Habib, Hassan Waqas, Iskander Tlili, M. Ijaz Khan, Waqar Azeem Khan, Unsteady transient slip flow of Williamson nanofluid containing gyrotactic microorganism and activation energy. Alex Eng J. 2020;59(6):4315–28.
[37] Ali M, Shahzad M, Sultan F, Khan WA, Rashid S. Exploring the features of stratification phenomena for 3D flow of Cross nanofluid considering activation energy. Int Commun Heat Mass Transf. 2020;116:104674.
[38] Khan SU, Waqas H, Muhammad T, Imran M, Aly S. Simultaneous effects of bioconvection and velocity slip in three-dimensional flow of Eyring-Powell nanofluid with Arrhenius activation energy and binary chemical reaction. Int Commun Heat Mass Transf. 2020;117:104738.
[39] Khan MI, Alzahrani F, Hobiny A, Ali Z. Estimation of entropy generation in Carreau-Yasuda fluid flow using chemical reaction with activation energy. J Mater Res Technol. 2020;9(5):9951–64.
[40] Naganthran K, Zeeshan A, Md Basir MdF, Shehzad N, Nazar R, Choudhary R et al. Concentration Flux Dependent on Radiative MHD Casson Flow with Arrhenius Activation Energy: Homotopy Analysis Method (HAM) with an Evolutionary Algorithm. Int J Heat Technol. 2020;38(4):785-793, 2020. https://doi.org/10.18280/ijht.380403.
[41] Waqas H, Farooq U, Ibrahim A, Shah Z, Kumam P. Numerical Simulation of Bioconvectional flow of Burger Nanofluid with effects of Activation energy and Exponential Heat Source/Sink over an Inclined Wall under the Swimming Microorganisms. Sci Rep. 2021. https://doi.org/10.21203/rs.3.rs-146009/v1.
[42] Dawar A, Islam S, Shah Z, Kumam P. Significance of Mixed Convection and Arrhenius Activation Energy in a Non-Newtonian Third Grade Fluid Flow Containing Gyrotactic Microorganisms towards Stretching Surface, *Scientific Reports*, 2021. https://doi.org/10.21203/rs.3.rs-146062/v1.
[43] Wang CY. Free convection on a vertical stretching surface [ZAMM] J Appl Math Mech. 1989;69:418–20.
[44] Gorla RS, Sidawi I. Free convection on a vertical stretching surface with suction and blowing. Appl Sci Res. 1994;52(3):247–57.
[45] Khan WA, Pop I. Boundary-layer flow of a nanofluid past a stretching sheet. Int J Heat Mass Transf. 2010;53(11-12):2477–83.
[46] Shampine LF, Gladwell I, Thompson S. Solving ODEs with MATLAB. New York: Cambridge University Press; 2003.

https://doi.org/10.1017/CBO9780511615542.
[47] Ibrahim W. Passive control of nanoparticle of micropolar fluid past a stretching sheet with nanoparticles, convective boundary condition and second-order slip. Proc IMechE Part E: J Process Mechanical Engineering. 2017;231(4):704–19.